START PAGE

Chapter 10

SYNCHRONOUS MOTORS FOR DRIVES

10.1. INTRODUCTION

Synchronous motors (SMs) are, in general, three-phase AC fed in the stator and DC (or PM) excited in the rotor. As the stator currents produce an m.m.f. traveling at the electric speed ω_1

$$\omega_1 = 2\pi f_1, \tag{10.1}$$

the rotor m.m.f. (or PM) is fixed to the rotor. The rotor electrical speed ω_r is

$$\omega_r = \omega_1 = 2\pi np, \tag{10.2}$$

in order to obtain two m.m.f. waves at standstill with each other. It is a known fact that only in this situation is a nonzero average torque per revolution obtained.

Yet, in an alternative interpretation, nonzero average torque is produced when the magnetic coenergy in the machine W_{co} varies with rotor position

$$T_e = \left(\frac{\partial W_{co}}{\partial \theta_r}\right)_{i_i = ct}; \quad \frac{d\theta_r}{dt} = \frac{\omega_r}{p} \tag{10.3}$$

θ_r is the geometrical rotor position angle.

Thus a magnetically anisotropic (reluctance) — exciterless — rotor may also be used. In all cases the number of pole pairs is the same on the stator and on the rotor.

PM or reluctance rotors are preferred, in general, for low (even medium) power motors (up to 50 - 300 kW in general) and excited rotors are used for medium and high power (hundreds of kW, MW and tens of MWs) applications.

As the SM speed is rigidly related to the stator frequency only the development of PECs — variable voltage and frequency sources — has made the SM suitable for variable speed drives.

The higher efficiency, power density and power levels per unit have thus become the main assets of variable speed synchronous motor drives.

10.2. CONSTRUCTION ASPECTS

As with any electrical motor, the SM has a stator and a rotor. The stator is made of a laminated core with uniform slotting. The stator slots

accommodate, in general, a three-phase, single- or double-layer winding made like for induction motors.

In general, the number of slots per pole and phase $q \geq 2$ and thus the coupling inductances vary sinusoidally with rotor position. However, in small power PM-SMs, concentrated windings may be used (q = 1 slot per pole per phase) when the sinusoidality is lost [1,2].

On the other hand, the SM rotors may be:

- active: - excited
  - with PMs
- passive: - highly anisotropic (variable reluctance)

The excited and PM rotors may be with salient or nonsalient poles, that is magnetically anisotropic or isotropic.

Also excited-rotor SMs may have a squirrel cage on the rotor to reduce the commutation inductance in current source PEC variable speed drives.

Figure 10.1 shows salient pole SMs with excited and PM rotors while Figure 10.2 exhibits nonsalient pole SMs.

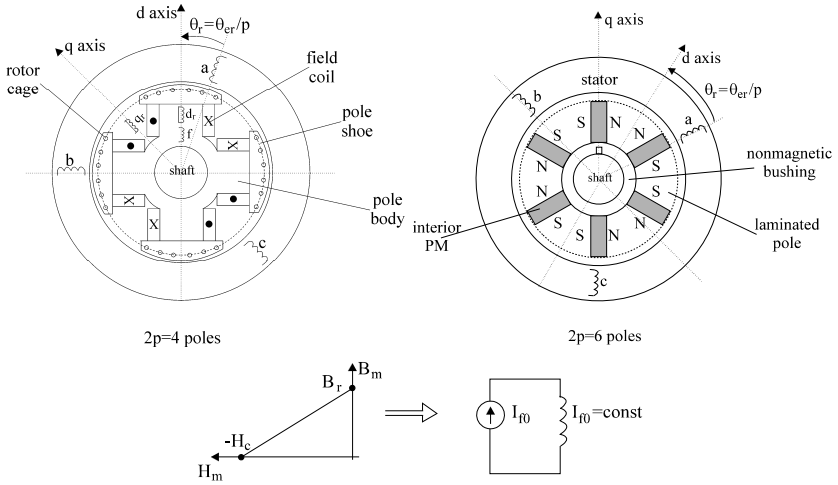

Figure 10.1. Salient pole active rotor SMs with a.) excited rotor, b.) interior PMs

The high energy PMs have a rather linear demagnetization characteristic in the second quadrant (Figure 10.1b) and thus such PMs may be considered as constant current ideal field coils or artificial superconducting coils at room temperature.

Once magnetized with a few high current pulses (milliseconds long), capable to produce (2 to 3) H_c and (2 to 3) B_r (see Figure 10.1), the magnetic energy stored in the PMs stays there for years if accidental demagnetization through ultrahigh stator currents is avoided.

The energy required to magnetize the PMs is much smaller than the power losses in an equivalent field winding over the active life of the PMs (4-5 years or more). However, the cost of PMs is notably higher than the

field winding costs. If the capitalized cost of losses is considered however, the extra cost of PMs is paid back in less than 2-3 years.

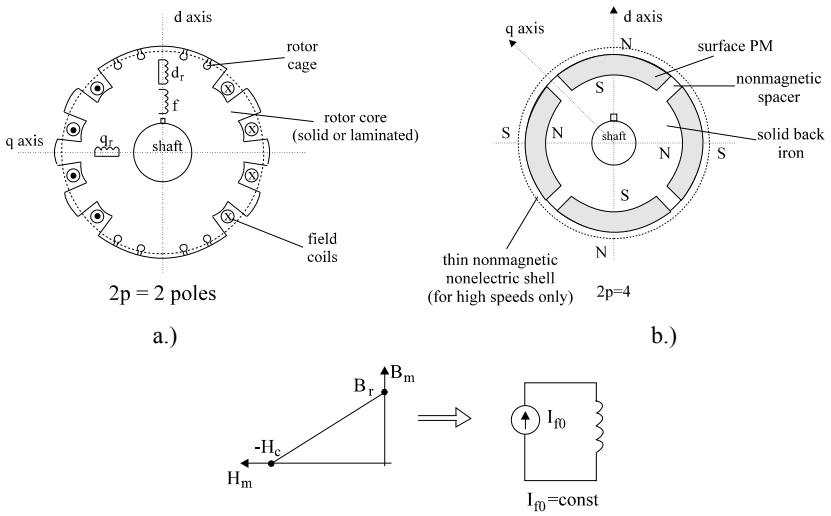

Figure 10.2. Nonsalient pole active rotors of SMs: a.) excited, b.) with surface PM

While the nonsalient pole configuration is more suitable for high peripheral speeds for excited rotors, with PM rotors the opposite is true; that is, interior PMs are, in general, preferred for high speed as PM "protection" against large centrifugal and radial electromagnetic forces are implicitly provided. Radial — attraction — forces between the PM rotor and the stator core are exerted through the surface PMs and through the laminated poles (for the interior PM rotors). Note that all PMs are rather severely temperature limited (100°C for NdFeB, 150°C for $SmCo_5$, etc) and thus, in adverse environments, the PMs are a liability.

Passive rotors are characterized by high magnetic anisotropy (or saliency). They may be made of conventional or of axial laminations (Figure 10.3a, b). Multiple flux barriers are provided to increase the saliency for the conventional rotor (Figure 10.3a). The same scope is served easily by alternating axial laminations with insulation layers (Figure 10.3b).

Special measures need to be taken to reduce the rotor core harmonics losses in the axially laminated anisotropic rotor [3].

Saliency ratios (for rated conditions) above 10 to 1 have been obtained, thus pushing the performance of reluctance synchronous motors (RSMs) to the level of IMs [3]. Obviously the absence of the rotor cage makes both PM-SMs and RSMs fully dependent on power electronic converters (PECs).

The insulation layers may be replaced by PMs along q axis (Figure 10.3b), in order to improve the torque density. Also, in the presence of a rotor cage on both PM rotor or variable reluctance rotor, the same motors

may be line-started and could operate at constant speed for constant voltage-frequency conditions.

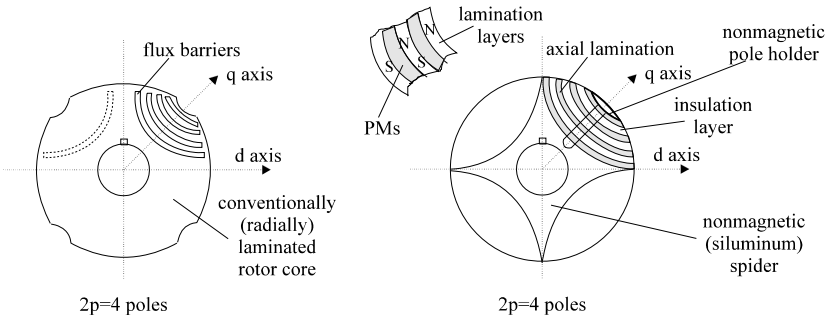

Figure 10.3. Passive-anisotropic (reluctance)-rotors for SMs: a.) multiple flux barrier rotor, b.) axially-laminated-anisotropic (ALA) rotor

10.3. PULSATING TORQUE

It is a known fact that an ideal SM, with sinusoidal m.m.f. and constant airgap — when fed with sinusoidal symmetric currents in the stator at frequency $\omega_1 = \omega_r$ (ω_r - rotor speed) — produces a constant torque.

In reality, pulsating torques may occur due to:

a. stator (and rotor) slot openings;

b. magnetic saturation caused by flux harmonics;

c. current waveforms;

d. PM field pulsations due to stator slot openings (cogging torque).

Items a to c cause the so-called electromagnetic pulsating torques while d causes the zero stator current (or cogging) torque.

Rotor pole (or PM) span correlation with stator slot openings, stator slot inclination or PM pole inclination, fractional q (slots per pole and phase) and, finally, special current waveform shaping through PEC control are all methods to reduce these, basically reluctance, parasitic torques [4] to less than 1% of rated torques. High performance smooth torque drives capable of operating below 20 rpm in sensorless control or under 1 rpm with position sensor control are thus obtained.

Note: Pulsating torque investigation requires, in most cases, FEM analysis - two-, quasi-two or three-dimensional [4].

10.4. THE PHASE COORDINATE MODEL

The phase coordinate model is based on phase equations using stator and rotor circuits. For $q \geq 2$ (slots per pole per phase) - distributed windings - the inductance matrix contains sinusoidal terms. We will take the case of the

salient pole rotor as the nonsalient pole rotor is a particular case of the former.

The phase inductance matrix [L] is (see Figures 10.1 and 10.2)

$$[L]=\begin{bmatrix} & a & b & c & f & d_r & q_r \\ a & L_{aa} & L_{ab} & L_{ac} & L_{af} & L_{ad_r} & L_{aq_r} \\ b & L_{ab} & L_{bb} & L_{bc} & L_{bf} & L_{bd_r} & L_{bq_r} \\ c & L_{ac} & L_{bc} & L_{cc} & L_{cf} & L_{cd_r} & L_{cq_r} \\ f & L_{af} & L_{bf} & L_{cf} & L_{ff} & L_{fd_r} & 0 \\ d_r & L_{ad_r} & L_{bd_r} & L_{cd_r} & L_{fd_r} & L_{d_rd_r} & 0 \\ q_r & L_{aq_r} & L_{bq_r} & L_{cq_r} & 0 & 0 & L_{q_rq_r} \end{bmatrix} \tag{10.4}$$

For distributed windings ($q \geq 2$) all the stator self, mutual, and stator-rotor inductances are rotor position, θ_{er}, dependent

$$\begin{aligned} L_{aa} &= L_{sl} + L_0 + L_2\cos 2\theta_{er} \\ L_{bb} &= L_{sl} + L_0 + L_2\cos(2\theta_{er} + 2\pi/3) \\ L_{cc} &= L_{sl} + L_0 + L_2\cos(2\theta_{er} - 2\pi/3) \\ L_{bc} &= -L_0/2 + L_2\cos 2\theta_{er} \\ L_{ac} &= -L_0/2 + L_2\cos(2\theta_{er} + 2\pi/3) \\ L_{ab} &= -L_0/2 + L_2\cos(2\theta_{er} - 2\pi/3) \end{aligned} \tag{10.5}$$

$$L_{ad_r} = L_{sd_r}\cos\theta_{er},\ L_{bd_r} = L_{sd_r}\cos(\theta_{er} - 2\pi/3),$$
$$L_{cd_r} = L_{sd_r}\cos(\theta_{er} + 2\pi/3)$$
$$L_{af} = L_{sf}\cos\theta_{er},\ L_{bf} = L_{sf}\cos(\theta_{er} - 2\pi/3),$$
$$L_{cf} = L_{sf}\cos(\theta_{er} + 2\pi/3)$$
$$L_{aq_r} = -L_{sq_r}\sin\theta_{er},\ L_{bq_r} = -L_{sq_r}\sin(\theta_{er} - 2\pi/3),$$
$$L_{cq_r} = -L_{sq_r}\sin(\theta_{er} + 2\pi/3)$$

Rotor inductances are evidently independent of rotor position as the saliency is on the rotor itself

$$\begin{aligned} L_{ff} &= L_{fl} + L_{fm} \\ L_{d_rd_r} &= L_{d_rl} + L_{d_rm},\ L_{q_rq_r} = L_{q_rl} + L_{q_rm} \end{aligned} \tag{10.6}$$

where $L_{fl}, L_{d_rl}, L_{q_rl}$ are leakage inductances while the others are related to main flux path.

On the other hand, for *concentrated* windings ($q = 1$), when nonsalient pole PM rotors are used, all stator inductances are independent of rotor position, the rotor cage is eliminated.

Only the motion-related inductances between the constant field-current PM equivalent circuit and the stator windings depend on rotor position.

$$[L]_{\substack{PM\\q=1}} = \begin{bmatrix} L_s & L_{ab} & L_{ab} & L_{af}(\theta_{er}) \\ L_{ab} & L_s & L_{ab} & L_{bf}(\theta_{er}) \\ L_{ab} & L_{ab} & L_s & L_{cf}(\theta_{er}) \\ L_{af}(\theta_{er}) & L_{bf}(\theta_{er}) & L_{cf}(\theta_{er}) & 0 \end{bmatrix} \tag{10.7}$$

The stator self-inductance L_s and the stator-stator mutual inductances L_{ab} are all equal to each other but different from $-L_0 / 2$ (as they would become for nonsalient rotors ($L_2 = 0$)). To a first approximation, $L_{ab} = -L_0 / 3$ [1].

The voltage-current matrix equation in phase coordinates (stator coordinates for stator, rotor coordinates for rotor) are

$$[V] = [r] \cdot [i] + \frac{d[\lambda]}{dt} \tag{10.8}$$

with

$$[\lambda] = \left[L(\theta_{er})\right] \cdot [i] \tag{10.9}$$

$$[i] = \left[i_a, i_b, i_c, i_{f_0}\right] \tag{10.10}$$

$$[r] = \text{Diag}[r_s, r_s, r_s, 0] \tag{10.11}$$

$$[\lambda] = [\lambda_a, \lambda_b, \lambda_c, 0] \tag{10.12}$$

Finally, the electromagnetic torque T_e may be calculated from the coenergy derivative with respect to rotor position

$$T_e = \frac{dW_{co}}{d(\theta_{er})} = \frac{d}{d(\theta_{er})} \int_0^{[i]} [\lambda] d[i]^T \tag{10.13}$$

After neglecting magnetic saturation, we multiply (10.8) by $[i]^T$

$$[i]^T \cdot [V] = [r] \cdot [i] \cdot [i]^T + \frac{d}{dt}\left(\frac{1}{2}[L] \cdot [i] \cdot [i]^T\right) + \\ + \frac{1}{2} \cdot [i]^T \cdot \frac{\partial}{\partial(\theta_{er})}\left[L(\theta_{er})\right] \cdot [i] \cdot \frac{d(\theta_{er})}{dt} \tag{10.14}$$

The last term is the electromagnetic power P_{elm}

$$T_e = \frac{P_{elm} \cdot p}{\omega_r} = \frac{p}{2} \cdot [i]^T \cdot \frac{\partial}{\partial \theta_{er}}\left[L(\theta_{er})\right] \cdot [i] \tag{10.15}$$

The motion equations are

$$\frac{J}{p}\frac{d\omega_r}{dt} = T_e - T_{load};\quad \frac{d(\theta_{er})}{dt} = \frac{\omega_r}{p} \tag{10.16}$$

As for the induction motor, we ended up with a set of eight nonlinear differential equations with time varying coefficients (basically, inductances). As such, these equations are used for special cases for machines with some asymmetry or for unbalanced supply voltage operation.

Also, for the concentrated stator winding (q = 1) and the PM nonsalient cageless rotor, the phase variable model is the only one to be used as $L_{af}(\theta_{er})$, $L_{bf}(\theta_{er})$ and $L_{cf}(\theta_{er})$ are far from sinusoidal functions. In order to get rid of the inductance dependence on rotor position for q ≥ 2, the space-phasor (d-q) model is used.

10.5. THE SPACE-PHASOR (d-q) MODEL

Proceeding as for the induction motor, we may define the stator current space-phasor, $\bar{i}_s$ in stator coordinates

$$\bar{i}_s^{\,s} = \frac{2}{3}\cdot\left(i_a + a\cdot i_b + a^2\cdot i_c\right) \tag{10.17}$$

On the other hand, from (10.9) with (10.4), the phase a flux linkage λ_a is

$$\lambda_a = L_{aa}i_a + L_{ab}i_b + L_{ac}i_c + L_{af}i_f + L_{ad_r}i_{d_r} + L_{aq_r}i_{q_r} \tag{10.18}$$

Making use of the inductance definition of (10.5) we find

$$\lambda_a = L_{sl}\,\mathrm{Re}\left(\bar{i}_s\right) + \frac{3}{2}L_0\,\mathrm{Re}\left(\bar{i}_s\right) + \frac{3}{2}L_2\,\mathrm{Re}\left(\bar{i}_s^{\,*}e^{2j\theta_{er}}\right) +$$
$$L_{af}\,\mathrm{Re}\left(i_f^{\,r}e^{j\theta_{er}}\right) + L_{sd_r}\,\mathrm{Re}\left(i_{d_r}^{\,r}e^{j\theta_{er}}\right) - \mathrm{Re}\left(jL_{sq_r}\,i_{q_r}^{r}e^{j\theta_{er}}\right) \tag{10.19}$$

The stator flux space-phasor $\bar{\lambda}_s$ is

$$\bar{\lambda}_s^{\,s} = \frac{2}{3}\left(\lambda_a + a\lambda_b + a^2\lambda_c\right) \tag{10.20}$$

Making use of (10.18) for λ_b, λ_c, (10.20) yields

$$\bar{\lambda}_s^{\,s} = L_{sl}\bar{i}_s^{\,s} + \frac{3}{2}L_0\bar{i}_s^{\,s} + \frac{3}{2}L_2\bar{i}_s^{\,s*}e^{2j\theta_{er}} +$$
$$L_{sf}i_f^{\,r}e^{j\theta_{er}} + L_{sd_r}i_{d_r}^{\,r}e^{j\theta_{er}} + L_{sq_r}ji_{q_r}^{\,r}e^{j\theta_{er}} \tag{10.21}$$

Multiplying (10.21) by $e^{-j\theta_{er}}$ we obtain

$$\bar{\lambda}_s{}^s e^{-j\theta_{er}} = \left(L_{sl} + \frac{3}{2}L_0\right)\bar{i}_s{}^s e^{-j\theta_{er}} + \frac{3}{2}L_2\left(\bar{i}_s{}^s e^{-j\theta_{er}}\right)^* + \\ + L_{sf} i_f{}^r + L_{sd_r} i_{d_r}{}^r + jL_{sq_r} i_{q_r}{}^r \tag{10.22}$$

We should now note that

$$\bar{\lambda}_s = \bar{\lambda}_s{}^s e^{-j\theta_{er}}; \quad \bar{i}_s = \bar{i}_s{}^s e^{-j\theta_{er}} \tag{10.23}$$

are space-phasors in rotor coordinates (aligned with rotor d axis).

With (10.23), (10.22) becomes

$$\bar{\lambda}_s = \left(L_{sl} + \frac{3}{2}L_0\right)\bar{i}_s + \frac{3}{2}L_2\bar{i}_s{}^* + L_{sf} i_f{}^r + L_{sd_r} i_{d_r}{}^r + jL_{sq_r} i_{q_r}{}^r \tag{10.24}$$

Next, the stator-phase equations in stator coordinates are

$$r_s i_a - V_a = -\frac{d\lambda_a}{dt}$$
$$r_s i_b - V_b = -\frac{d\lambda_b}{dt}$$
$$r_s i_c - V_c = -\frac{d\lambda_c}{dt} \tag{10.25}$$

We may translate them in space-phasors as

$$r_s \bar{i}_s{}^s - \bar{V}_s{}^s = -\frac{d\bar{\lambda}_s{}^s}{dt} = -\frac{d}{dt}\left(\bar{\lambda}_s e^{j\theta_{er}}\right) = -e^{j\theta_{er}}\frac{d\bar{\lambda}_s}{dt} - j\omega_r \bar{\lambda}_s e^{j\theta_{er}} \tag{10.26}$$

The final form of (10.26) is

$$r_s \bar{i}_s - \bar{V}_s = -\frac{d\bar{\lambda}_s}{dt} - j\omega_r \bar{\lambda}_s; \quad \omega_r = \frac{d\theta_{er}}{dt} \tag{10.27}$$

and

$$V_0 = r_s i_0 + L_{sl}\frac{di_0}{dt}; \quad i_0 = \left(i_a + i_b + i_c\right)/3 \tag{10.28}$$

Equation (10.27) is, in fact, identical to that for the induction machine. Only the flux expression (10.24) is different.

$$\bar{\lambda}_s = \lambda_d + j\lambda_q; \quad \lambda_d = L_{sl} i_d + \lambda_{dm}; \quad \lambda_{dm} = L_{dm} i_d{}^r + L_{sf} i_f{}^r + L_{sd} i_{d_r}{}^r \tag{10.29}$$

$$\lambda_q = L_{sl} i_q + \lambda_{qm}; \quad \lambda_{qm} = L_{qm} i_d + L_{sq} i_{q_r}{}^r \tag{10.30}$$

$$L_{dm} = \frac{3}{2}\left(L_0 + L_2\right)$$

with
$$L_{qm} = \frac{3}{2}\left(L_0 - L_2\right) \tag{10.31}$$

L_{dm} and L_{qm} are called the d-q magnetizing inductances.

We may reduce the rotor to stator currents

$$\frac{i_f}{i_f^{\,r}} = \frac{L_{sf}}{L_{dm}} = K_f;\quad \frac{i_{d_r}}{i_{d_r}^{\,r}} = \frac{L_{sd}}{L_{dm}} = K_d;\quad \frac{i_{q_r}}{i_{q_r}^{\,r}} = \frac{L_{sq}}{L_{dm}} = K_q; \tag{10.32}$$

$$\lambda_{dm} = L_{dm} i_{dm};\quad i_{dm} = i_d + i_f + i_{d_r}$$

$$\lambda_{qm} = L_{qm} i_{qm};\quad i_{qm} = i_q + i_{q_r};\quad i_m = \sqrt{i_{dm}^{\,2} + i_{qm}^{\,2}} \tag{10.33}$$

Magnetic saturation may be determined by unique $\lambda_{dm}(i_m)$ and $\lambda_{qm}(i_m)$ functions to be either calculated or measured [5].

The stator equation (10.27) in d-q coordinates becomes

$$V_d = r_s i_d + \frac{d\lambda_d}{dt} - \omega_r \lambda_q \tag{10.34}$$

$$V_q = r_s i_q + \frac{d\lambda_q}{dt} + \omega_r \lambda_d \tag{10.35}$$

Now we should add the rotor equations in rotor d-q coordinates (as along axes d and q, the rotor windings are not at all symmetric)

$$V_f = r_f i_f + \frac{d\lambda_f}{dt};\quad \lambda_f = L_{fl} i_f + \lambda_{dm} \tag{10.36}$$

$$0 = r_{d_r} i_{d_r} + \frac{d\lambda_{d_r}}{dt};\quad \lambda_{d_r} = L_{d_r l} i_{d_r} + \lambda_{dm} \tag{10.37}$$

$$0 = r_{q_r} i_{q_r} + \frac{d\lambda_{q_r}}{dt};\quad \lambda_{q_r} = L_{q_r l} i_{q_r} + \lambda_{qm} \tag{10.38}$$

The torque, T_e, is

$$T_e = \frac{3}{2} p\, \mathrm{Re}\left(j\bar{\lambda}_s \bar{i}_s^{\,*}\right) = \frac{3}{2} p\left(\lambda_d i_q - \lambda_q i_d\right) \tag{10.39}$$

Finally, the d-q variables are related to the abc variables by the Park transformation

$$\overline{V}_s = V_d + jV_q = \frac{2}{3}\left(V_a + aV_b + a^2 V_c\right)e^{-j\theta_{er}};\quad a = e^{j2\pi/3} \tag{10.40}$$

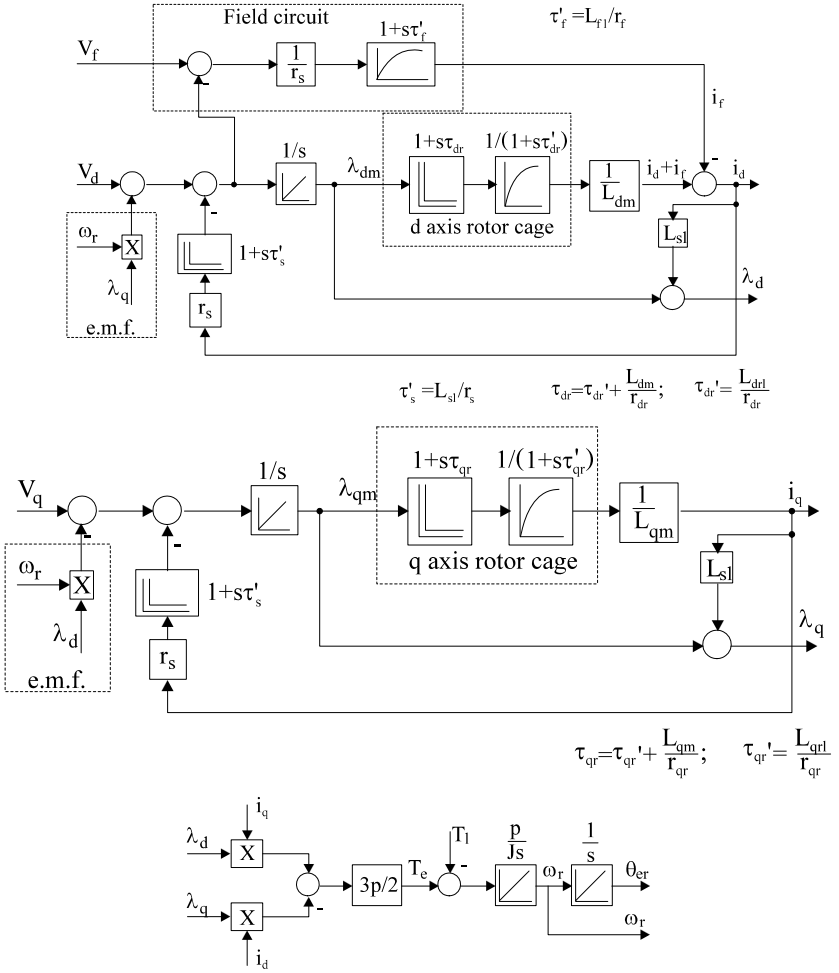

Figure 10.4. Signal flow diagram of SMs

Note also that all rotor variables are reduced to the stator

$$V_f = V_f^{\,r}/K_f;\quad r_f = r_f^{\,r}/K_f^{\,2};\quad L_{fl} = L_{fl}^{\,r}/K_f^{\,2} \tag{10.41}$$

$$r_{dr} = r_{dr}^{\,r}/K_d^{\,2};\quad L_{drl} = L_{drl}^{\,r}/K_d^{\,2} \tag{10.42}$$

$$r_{qr} = r_{qr}^{\,r}/K_q^{\,2};\quad L_{qrl} = L_{qrl}^{\,r}/K_q^{\,2} \tag{10.43}$$

The motion equations (10.16) are to be added.

The d-q model is also of 8th order and basically nonlinear, but the coefficients are position (time) independent. The signal flow diagram of the d-q model is shown in Figure 10.4.

PM or reluctance rotor SMs used for variable speed lack the excitation winding and i_f = const. (zero for RSM).

They also lack the damper cage ($\tau_{dr} = \tau_{rd}' = \tau_{qr} = \tau_{qr}' = 0$) (Figure 10.5).

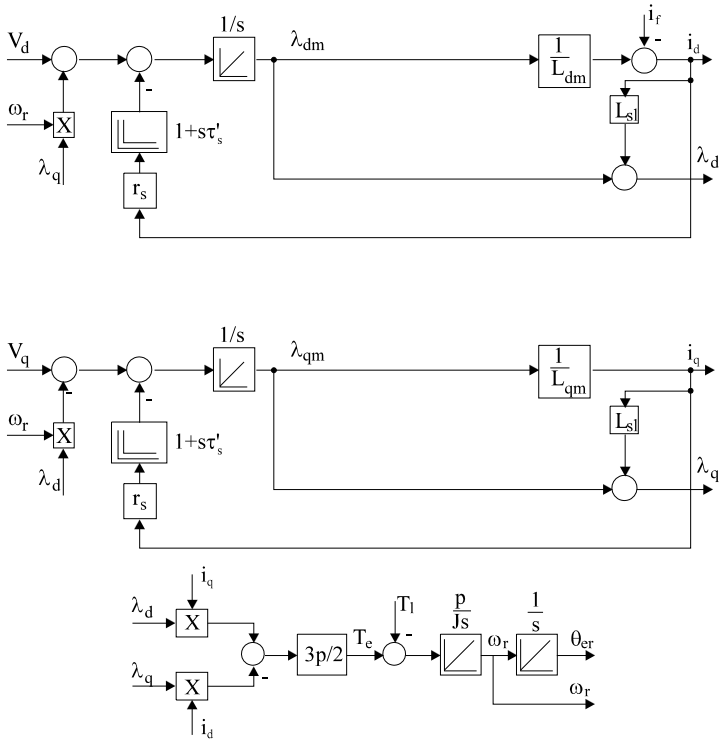

Figure 10.5. Flow signal diagram of PM and reluctance SMs (no rotor damper cage)

The signal flow diagrams may be arranged into equivalent circuits (Figure 10.6).

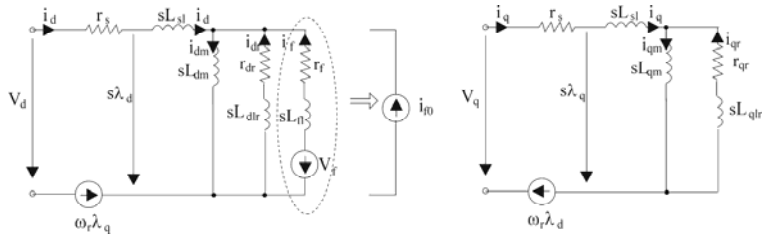

Figure 10.6. SM equivalent circuits

For the PM-SM (Figure 10.6), the field winding circuit is replaced by an ideal (constant) current source i_{f0}; $i_{f0} = 0$ for the RSM.

Finally, for the cageless rotor, $r_{dr} = r_{qr} = \infty$ ($i_{dr} = i_{qr} = 0$). For steady-state, simply s = 0 as we will demonstrate in the following section.

10.6. STEADY-STATE OPERATION

For steady-state the stator phase voltages are given by

$$V_{abc} = \sqrt{2}V\cos\left[\omega_1 t - (i-1)\frac{2\pi}{3}\right];\quad i = 1,2,3 \tag{10.44}$$

where ω_1 = const., and thus the rotor position θ_{er} is

$$\theta_{er} = \int \omega_r dt = \int \omega_1 dt = \omega_1 t + \theta_0 \tag{10.45}$$

Note that $\omega_r = \omega_{r0} = \omega_1$ for steady-state.

Using (10.40) the d-q voltage components V_d, V_q in rotor coordinates are

$$\overline{V}_s = V_d + jV_q = V\sqrt{2}\cos\theta_0 - jV\sqrt{2}\sin\theta_0 \tag{10.46}$$

As V_d, V_q are time independent so will be the currents in the stator i_d, i_q. Also d/dt = 0 (s = 0) and thus from (10.38), $i_{d_r} = i_{q_r} = 0$ (zero damper cage currents) and $i_f = i_{f0} = V_f / r_f$ = const.

The space-phasor diagram follows from ((10.34)-(10.35)) which may be written in space-phasor form as the stator is symmetric electrically and magnetically (Figure 10.7).

$$\overline{V}_s = r_s\bar{i}_s + j\omega_r\overline{\lambda}_s;\ \omega_r = \omega_1 \tag{10.47}$$

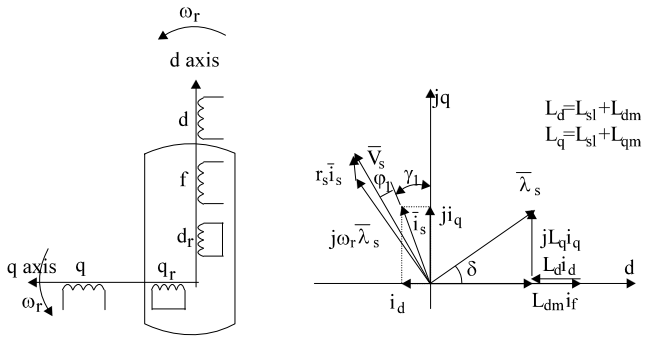

a.) b.)

Figure 10.7. SM - steady-state - with excitation or PMs a.) d-q axis model, b.) space-phasor diagram

For steady-state all variables in the space-phasor (or d-q) model are DC quantities. Space angles translate into time-phase shift angles between stator quantities (like φ_1 - the power factor angle) in phase coordinates.

Using the d-q model for speed control is thus ideal, as steady-state means DC

10.7. TO VARY SPEED VARIABLE FREQUENCY IS MANDATORY

SMs keep a tight relationship between speed and frequency as the rotor m.m.f. (if any) is of DC (or PM) character

$$n = f_1 / p; \quad \omega_r = \omega_1; \quad \Omega_r = \omega_r / p \tag{10.48}$$

Varying the number of pole pairs p is unusual so, in fact, to vary speed variable frequency is mandatory. How to vary frequency in relation to stator voltage V_s and field current i_f (or voltage V_{ex}) — if any — to obtain steady-state and (or) transient performance suitable for various applications is the key to SM drives control.

While this problem will be dealt with in detail in the following chapters, the main principles will be illustrated through three numerical examples.

Example 10.1. Unity power factor and constant stator flux.

Let us consider an excited synchronous motor with the data: $V_n = 660V$ (line voltage, rms, star connection), $I_n = 500/\sqrt{2}$ (rms), $r_s = 0.016\Omega$, $L_d = 2L_q = 0.0056H$, $L_{sl} = 0.1L_d$, $\omega_1 = 2\pi 60 rad/s$, p = 2 pole pairs.

Determine:

- The steady-state space-phasor diagram for unity power factor ($\varphi_1 = 0$)
- Calculate the values of i_f, i_d, i_q for unity power factor and rated phase current, I_n.
- Calculate the torque for $\varphi_1 = 0$.
- Derive and plot the torque/speed curve for rated and half-rated stator flux for variable frequency and constant stator voltage.

Solution:

a. The required space-phasor diagram comes from Figure 10.7b with φ_1=0.

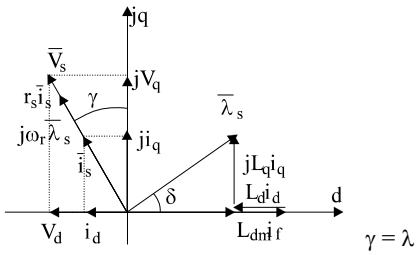

Figure 10.8. Space-phasor diagram for unity power factor

b. From Figure 10.8 we have

$$V_s = r_s i_s + \omega_r \lambda_s \tag{10.49}$$

$$\bar{\lambda}_s = \lambda_d + j\lambda_q = L_d i_d + L_{dm} i_f + jL_q i_q \tag{10.50}$$

For no-load

$$V_{s0} = \omega_r L_{dm} i_f;\ \ \left(i_d = i_q = 0\right);\ \ \omega_r = \omega_1 \tag{10.51}$$

$$V_s = \frac{660\sqrt{2}}{\sqrt{3}} = 537.92\,\text{V};\ \ i_s = i_n\sqrt{2} = \frac{500}{\sqrt{2}}\sqrt{2} = 500\,\text{A} \tag{10.52}$$

From (10.49) the rated stator flux λ_s is

$$\lambda_s = \frac{V_s - r_s i_s}{\omega_r} = \frac{537.92 - 0.016 \cdot 500}{2\pi 60} = 1.406 \text{ Wb} \tag{10.53}$$

$$i_q = i_s \cos\delta \tag{10.54}$$

$$L_q i_q = \lambda_s \sin\delta \tag{10.55}$$

Thus

$$\lambda_s \tan\delta = L_q i_s \tag{10.56}$$

$$\tan\delta = \frac{L_q i_s}{\lambda_s} = \frac{0.0028 \cdot 500}{1.406} \approx 1 \Rightarrow \delta = 45^0 \tag{10.57}$$

$$-i_d = i_q = \frac{i_s}{\sqrt{2}} = \frac{500}{\sqrt{2}} = 354.61 \text{ A} \tag{10.58}$$

$$\lambda_d = \lambda_q = \frac{\lambda_s}{\sqrt{2}} = \frac{1.406}{\sqrt{2}} = 0.997 \text{ Wb} \tag{10.59}$$

$$\lambda_d = L_d i_d + L_{dm} i_f \tag{10.60}$$

The field current i_f (reduced to the stator) is

$$i_f = \frac{\lambda_d - L_d i_d}{L_d - L_{sl}} = \frac{0.997 - 0.0056 \cdot (-354.61)}{0.0056(1 - 0.1)} = 591.82 \text{ A} \tag{10.61}$$

The electromagnetic torque T_e is

$$T_e = \frac{3}{2} p\left(\lambda_d i_q - \lambda_q i_d\right) =$$

$$= \frac{3}{2} \cdot 2 \cdot \left(0.997 \cdot 354.61 - 0.997 \cdot (-354.61)\right) = 2121 \text{ Nm} \tag{10.62}$$

Note that for $\cos\varphi_1 = 1$ the torque expression (10.39) may be written as

$$T_e = \frac{3}{2} p \lambda_s i_s \tag{10.63}$$

The stator flux and current space-phasors are rectangular, as in a DC motor. Consequently, for constant stator flux λ_s, the torque is proportional to stator current.

Varying the frequency $\omega_1 = \omega_r$, such that λ_s = const and $\cos\varphi_1 = 1$ appears as an optimum way to speed control.

The torque/speed curve may be derived from (10.49) with (10.63) by eliminating the stator current i_s

$$i_s = \frac{2T_e}{3p\lambda_s} \tag{10.64}$$

$$V_s = \omega_r \lambda_s + \frac{2r_s T_e}{3p\lambda_s} \tag{10.65}$$

As $\omega_1 = \omega_r$, varying speed means, implicitly, that the frequency changes.

The torque/speed curve is a straight line as in a separately excited DC brush motor. The ideal no-load speed ($T_e = 0$) ω_{r0} is

$$\omega_{r0} = \frac{V_s}{\lambda_s} \tag{10.66}$$

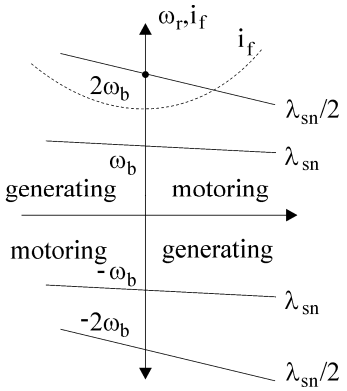

Figure 10.9. Speed/torque curves for constant flux and unity power factor

For rated flux and full voltage, V_{sn}, the base speed ω_b is obtained. Above the base speed, ω_{r0} may be modified only through flux weakening as in a DC brush motor. Halving the flux doubles the ideal no-load speed ω_{r0}. The torque speed curves are illustrated on Figure 10.9.

Four-quadrant operation is implicit as negative frequency $\omega_1 = \omega_r$ means negative order (a →c → b instead of a → b → c) of stator phases fed from a PEC.

Note that in order to maintain unity power factor, the field current has to be increased with torque (power) — Figure 10.9.

A tight coordination of stator and rotor currents control is required to maintain the above conditions, but once this is done — through vector control — ideal (linear) torque/speed curves are obtained.

Low speed, large power, SMs for cement mills or the like, fed from cycloconverters, operate, in general, under such conditions (Chapter 14).

Example 10.2. Leading power factor and constant stator flux.

Consider an excited SM with the same data as in example 10.1.

Determine:

- The steady-state-space-phasor diagram for a leading power factor angle $\varphi_1 = -12^\circ$;
- Calculate the values of i_f, i_d, i_q for rated current and $\varphi_1 = -12^\circ$.
- Calculate the stator flux λ_s, its components λ_d and λ_q and the corresponding electromagnetic torque T_e.
- Calculate the value of field current for half the rated torque and same (base) speed $\omega_b = 2\pi 60$ rad/s.
- Plot the torque/speed curve for rated and half-rated stator flux and $\varphi_1 = -12^\circ$.

Solution:

The space-phasor diagram of Figure 10.7b is redrawn with $\varphi_1 = -12^\circ$ (leading) as in Figure 10.10.

From Figure 10.10 we may write approximately

$$V_s \approx r_s i_s \cos\varphi_1 + \omega_r \lambda_s \tag{10.67}$$

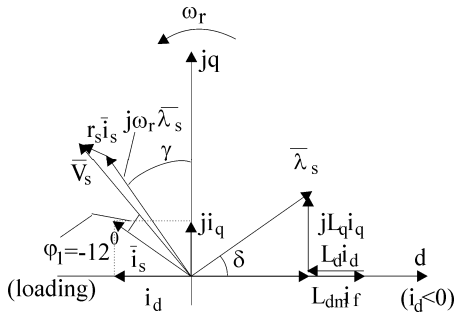

Figure 10.10. Leading power factor and constant stator flux

The torque T_e is

$$T_e = \frac{3}{2} p\,\mathrm{Re}\left(j\bar{\lambda}_s \bar{i}_s^*\right) = \frac{3}{2} p\lambda_s i_s \cos\delta \approx \frac{3}{2} p\lambda_s i_s \cos\varphi_1 \tag{10.68}$$

$$\lambda_s \approx \frac{V_s - r_s i_s \cos\varphi_1}{\omega_r} = \frac{537.92 - 500 \cdot 0.016 \cdot \cos(-12^\circ)}{2\pi 60} = 1.4068 \text{ Wb} \tag{10.69}$$

The corresponding torque T_e is

$$T_e = \frac{3}{2} \cdot 2 \cdot 1.4068 \cdot 500 \cdot 0.978 = 2063.83 \text{ Nm} \tag{10.70}$$

$$i_q \approx i_s \cos\left(\delta + |\varphi_1|\right) \tag{10.71}$$

$$L_q i_q = \lambda_s \sin\delta \tag{10.72}$$

Consequently,

$$\frac{\sin\delta}{\cos\left(\delta + |\varphi_1|\right)} = \frac{L_q i_s}{\lambda_s} = \frac{0.0028 \cdot 500}{1.4068} = 0.99 \tag{10.73}$$

$\delta = 39^0$ (it was 45^0 for $\cos\varphi_1 = 1$ in example 10.1)

Now
$$i_q = 500 \cdot \cos(39^\circ + 12^\circ) = 413.66 \text{ A} \tag{10.74}$$

$$i_d = -500 \cdot \sin(39^\circ + 12^\circ) = -388.57 \text{ A} \tag{10.75}$$

$$\lambda_q = L_q i_q = 0.0028 \cdot 314.66 = 0.881 \text{ Wb} \tag{10.76}$$

$$\lambda_d = \lambda_s \cos\delta = 1.4068 \cdot \cos 39^\circ = 1.09388 \text{ Wb} \tag{10.77}$$

Finally, from (10.58) the field current is obtained

$$i_f = \frac{\lambda_d - L_d i_d}{L_{dm}} = \frac{1.09388 - 0.0056 \cdot (-388.57)}{0.0056 \cdot 0.9} = 648.78 \text{ A} \tag{10.78}$$

This value has to be compared with i_f = 591.82A for $\cos\varphi_1 = 1$ in (10.61).

The torque/speed curve may be obtained from (10.67)-(10.68) under the form

$$V_s = \omega_r \lambda_s + \frac{2 r_s T_e}{3 p \lambda_s} \tag{10.79}$$

Thus the torque curve is quite similar to that of (10.65) for $\cos\varphi_1 = 1$.

The main difference is that for the same stator current, the same stator voltage and speed, we obtain slightly less torque and we need a higher field current to provide for leading power factor angle $\varphi_1 < 0$. This value of φ_1 =

$-12 < 0$ might be preserved for various loads if the field current is continuously adjusted. This type of coordinated frequency-stator flux-field current change method is currently used in high speed high power excited-rotor SM drives with current-source inverters. It will be detailed in the chapter dedicated to large power drives (Chapter 14).

Example 10.3. PM-SM, operation for constant i_d.

A nonsalient pole rotor PM-SM has the data: V_n = 180V (rms, line voltage, star connection of phases), $L_d = 0.4L_q = 0.05$H $r_s = 1\Omega$, no-load line voltage (rms) at n_n = 1500rpm (f_1 = 60Hz), V_{on} = 180V (rms).

Determine:

- The PM flux linkage λ_{PM};
- The torque/speed curve for $i_d = 0$, $i_d = \pm 5$A and the ideal no-load speed in the three cases, stator flux and torque for i_q = 10A;
- Draw d-q equivalent circuits for steady-state and introduce the iron losses in the model.

Solution:

The no-load voltage V_{on} "translated" into space-vector terms, V_{s0}

$$V_{s0} = \frac{V_{on}\sqrt{2}}{\sqrt{3}} = \frac{180\sqrt{2}}{\sqrt{3}} = 146.7 \quad \text{V} \tag{10.80}$$

According to (10.50)

$$\left(\lambda_d\right)_{i_d=0} = L_{dm} i_{f0} = \lambda_{PM} \tag{10.81}$$

$$\left(\lambda_q\right)_{i_q=0} = 0 \tag{10.82}$$

$$V_{s0} = \omega_r L_{dm} i_{f0} = \omega_r \lambda_{PM} \tag{10.83}$$

$$\lambda_{PM} = \frac{V_{s0}}{\omega_r} = \frac{146.70}{2\pi 60} = 0.389 \quad \text{Wb} \tag{10.84}$$

As

$$\lambda_d = L_d i_d + \lambda_{PM} \qquad \lambda_q = L_q i_q \tag{10.85}$$

the electromagnetic torque T_e is

$$T_e = \frac{3}{2} p\left(\lambda_d i_q - \lambda_q i_d\right) = \frac{3}{2} p\left[\lambda_{PM} + \left(L_d - L_q\right) i_d\right] i_q \tag{10.86}$$

The d-q voltage components ((10.34)-(10.35)), with d/dt = 0, are

$$\begin{aligned} V_d &= r_s i_d - \omega_r \lambda_q \\ V_q &= r_s i_q + \omega_r \lambda_d \end{aligned} \tag{10.87}$$

Now we replace i_q from (10.86) into (10.87). Thus we have

$$V_d^2 + V_q^2 = V_s^2 = r_s^2\left(i_d^2 + i_q^2\right) + 2\omega_r r_s\left(\lambda_d i_q - \lambda_q i_d\right) + \\ + \omega_r^2\left[\left(L_d i_d + \lambda_{PM}\right)^2 + \left(L_q i_q\right)^2\right] \tag{10.88}$$

or

$$V_s^2 = r_s^2 i_d^2 + \left(r_s^2 + \omega_r^2 L_q^2\right)\cdot\frac{4}{9}\frac{T_e^2}{p^2}\frac{1}{\left[\lambda_{PM} + \left(L_d - L_q\right)i_d\right]^2} + \\ + \frac{4}{3}\frac{\omega_r}{p} r_s T_e + \omega_r^2\left(L_d i_d + \lambda_{PM}\right)^2 \tag{10.89}$$

The ideal no-load ($T_e = 0$) speed ω_{r0} is

$$\omega_{r0} = \frac{\sqrt{V_s^2 - r_s^2 i_d^2}}{L_d i_d + \lambda_{PM}} \tag{10.90}$$

For $i_d = 0$

$$\left(\omega_{r0}\right)_{i_d=0} = \frac{V_{sn}}{\lambda_{PM}} = \frac{180\sqrt{2}}{0.389\sqrt{3}} = 377.13 \text{ rad/s} \tag{10.91}$$

Also,

$$\left(\omega_{r0}\right)_{i_d=-5A} = \frac{\sqrt{146.30^2 - (1.5)^2}}{\left(0.05\cdot(-5) + 0.389\right)} \approx 984 \text{ rad/s} \tag{10.92}$$

$$\left(\omega_{r0}\right)_{i_d=5A} = \frac{\sqrt{146.30^2 - (1.5)^2}}{\left(0.05\cdot 5 + 0.389\right)} \approx 229 \text{ rad/s} \tag{10.93}$$

Note that $i_d < 0$ means a demagnetizing effect. However, the torque expression (10.86) shows that as $L_d < L_q$ only $i_d < 0$ produces a positive torque contribution.

A positive torque contribution for $i_d < 0$ is accompanied by a reduction in the stator flux as

$$\left(\lambda_s\right)_{\substack{i_q=0\\ i_d=-5A}} = \lambda_d = L_d i_d + \lambda_{PM} = -0.05\cdot 5 + 0.389 = 0.149 \text{ Wb} \tag{10.94}$$

$$\left(\lambda_s\right)_{\substack{i_q=0\\ i_d=5A}} = 0.05\cdot 5 + 0.389 = 0.639 \text{ Wb} \tag{10.95}$$

The torque for $i_d = 0, -5A, +5A$, $i_q = 10A$ is

$$\left(T_e\right)_{\substack{i_d=0\\ i_q=10A}} = \frac{3}{2} p\lambda_{PM} i_q = \frac{3}{2}\cdot 2\cdot 0.389\cdot 10 = 11.67 \text{ Nm} \qquad (10.96)$$

$$\left(T_e\right)_{\substack{i_d=-5A\\ i_q=10A}} = \frac{3}{2}\cdot 2\cdot\left(0.389+(0.05-0.125)\cdot\left(-5\right)\right)\cdot 10 = 22.92 \text{ Nm} \qquad (10.97)$$

$$\left(T_e\right)_{\substack{i_d=5A\\ i_q=10A}} = \frac{3}{2}\cdot 2\cdot\left(0.389+(0.05-0.125)\cdot 5\right)\cdot 10 = 0.42 \text{ Nm} \qquad (10.98)$$

Positive i_d values are to be avoided as they increase the flux level and decrease the torque considerably.

The d-q equivalent circuits for steady-state (s = 0) reflect, in fact, Equations (10.87) - Figure 10.11.

Though the core losses are related to the main flux components we may assume them to be produced by the stator flux.

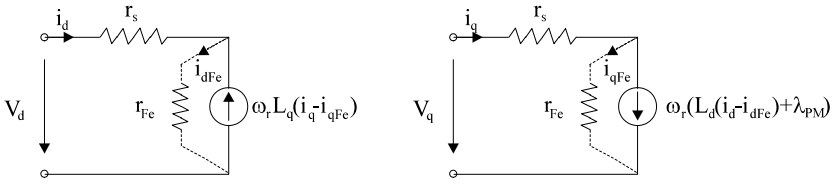

Figure 10.11. Steady-state d-q equivalent circuits of PM-SM with core losses included

The core losses occurring in the stator are considered produced in a resistance r_{Fe}, to be determined through measurements.

Now, with core losses included, Equations (10.87) are no longer strictly valid but they may be modified simply based on the equivalent circuit. Introduced in parallel with e.m.f.s, r_{Fe} should not vary dramatically with frequency.

Example 10.4. The reluctance synchronous motor (RSM) steady-state

A high performance RSM has the data: L_d = 10 L_q = 0.1 H, p = 2, r_s = 1Ω, f_1 = 60 Hz.

Determine:

a. The space-phasor diagram;

b. The maximum torque per given stator current and for given stator flux;

c. Introduce a PM along axis q to reduce the q axis flux. Draw the new space-phasor diagram and discuss it. Calculate the torque for i_d = 3A, i_q = 15A without and with PM flux $\lambda_{PM} = -L_q i_q$.

d. Calculate the stator flux to produce the respective torques.

Solution:

The space-phasor diagram is obtained simply from the general one (Figure 10.7) with $i_f = 0$ and $L_d >> L_q$ (Figure 10.12).

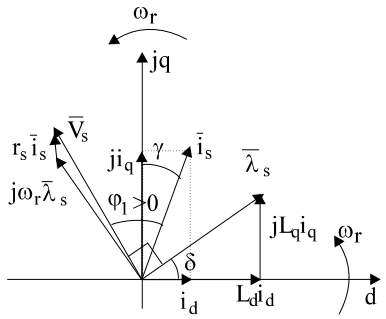

Figure 10.12. RSM - space-phasor diagram

The torque expression (10.86) with $i_f = 0$ and $L_d >> L_q$ is

$$T_e = \frac{3}{2}p\left(L_d - L_q\right)i_d i_q \tag{10.99}$$

The voltage equations (10.87) become

$$\begin{aligned} V_d &= r_s i_d - \omega_r L_q i_q \\ V_q &= r_s i_q + \omega_r L_d i_d \end{aligned} \tag{10.100}$$

The stator flux $\bar{\lambda}_s$ and stator current $\bar{i}_s$ are

$$\bar{\lambda}_s = \lambda_d + j\lambda_q = L_d i_d + jL_q i_q \tag{10.101}$$

$$\bar{i}_s = i_d + ji_q \tag{10.102}$$

The maximum torque for given stator current, i_s

$$i_s = \sqrt{{i_d}^2 + {i_q}^2} \tag{10.103}$$

may be obtained from (10.99) and (10.103)

$$\frac{\partial T_e}{\partial i_d} = 0 \tag{10.104}$$

After eliminating i_q we get

$$i_{di} = i_{qi} = i_s/\sqrt{2};\quad T_{ei} = \frac{3}{2}p\left(L_d - L_q\right)\frac{{i_s}^2}{2} \tag{10.105}$$

Consequently, $\gamma = 45°$ in Figure 10.12.

If $i_s = i_n$ (rated current) $i_{di} = i_{sn}/\sqrt{2}$ the machine is driven into heavy saturation as i_{di} is too high in comparison with the rated no-load phase current i_0, with the exception of very low power motors when $i_0 / i_n > 0.707$. Though it leads to maximum torque per ampere it may be used for torques lower than 50-60% of rated torque. This may be the case for low speed operation in some variable speed drive applications.

On the other hand, for given stator flux (10.101), the maximum torque is obtained for

$$i_{dk} L_d = i_{qk} L_q = \lambda_s / \sqrt{2} \tag{10.106}$$

The maximum torque is

$$T_{ek} = \frac{3}{2} p \left(L_d - L_q \right) \frac{\lambda_s^{\,2}}{2 L_d L_q} \tag{10.107}$$

This time the d-q flux angle is $\delta = 45°$ in Figure 10.12.

As it provides maximum torque per given flux, this is the limit condition at high speeds when the flux is limited (flux weakening zone).

Introducing the PM in axis q

$$\lambda_q = L_q i_q - \lambda_{PMq}; \quad \lambda_d = L_d i_d \tag{10.108}$$

In (10.108) $\lambda_{PMq} \geq L_q i_{q\,max}$ to avoid PM demagnetization. The torque expression (10.86) becomes

$$i_{dk} = i_{di} = i_0 / \sqrt{2}; \quad T_e = \frac{3}{2} p \left[\left(L_d - L_q \right) i_q + \lambda_{PM} \right] i_d \tag{10.109}$$

This time, to change the torque sign (for regenerative braking) the sign of i_d (rather than i_q) has to be changed in variable speed drives. The space-phasor diagram of PM-RSM is shown in Figure 10.13.

Note that for motoring $\delta < 0$ (the flux vector is lagging (not leading) the d axis) and the power factor has been increased, together with torque.

Only low remnant flux density (moderate cost) PMs are required as $L_q i_{sn}$ is still a small flux ($L_d / L_q >> 1$).

Let us now calculate the torque and stator flux for the two situations

$$\left(T_e \right)_{\lambda_{PM_q}=0} = \frac{3}{2} \cdot p \left(L_d - L_q \right) i_d i_q = \frac{3}{2} \cdot 2 \cdot 0.1 \cdot \left(1 - \frac{1}{10} \right) 3 \cdot 15 = 12.15 \text{ Nm} \tag{10.110}$$

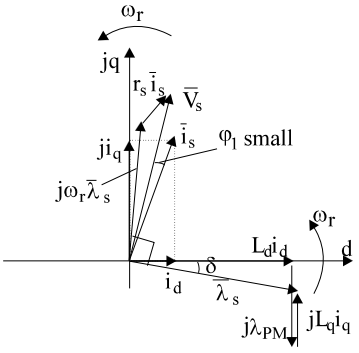

Figure 10.13. PM-SRM - space-phasor diagram

$$\lambda_s = \sqrt{L_d{}^2 i_d{}^2 + L_q{}^2 i_q{}^2} = \sqrt{0.1^2 \cdot 3^2 + \left(\frac{0.1}{10} \cdot 15\right)^2} = 0.335 \text{ Wb} \quad (10.111)$$

$$\left(T_e\right)_{\lambda_{PM_q} \neq 0} = \frac{3}{2} \cdot 2 \cdot \left(0.1 \cdot \left(1 - \frac{1}{10}\right) \cdot 15 + \frac{0.1}{10} \cdot 15\right) \cdot 3 = 13.15 \text{ Nm} \quad (10.112)$$

$$\lambda_s = L_d i_d = 0.1 \cdot 3 = 0.3 \text{ Wb} \quad (10.113)$$

So, the PMs in axis q produce almost a 10% torque increase for a 10% decrease in flux level.

The improvements are more spectacular in lower saliency machines (L_d / L_q = 5-8), which are easier to build.

10.8. COGGING TORQUE AND TOOTH-WOUND PMSMs

PMSMs develop a pulsating torque at zero stator current due to the PM magnetic coenergy variation with rotor position in the presence of stator slot openings.

This zero current torque which has a zero average value per 360° is called cogging torque.

Cogging torque stems from the PM airgap flux density variation due to stator slot openings and depends also on other factors such as:

- PM shape and placement
- The number of stator slots Ns and rotor poles 2p

Figure 10.14 shows the PM airgap flux density obtained from Finite Element Analysis (FEA) at the center of airgap for a 27 stator slot 6 rotor PM poles PMSM [6].

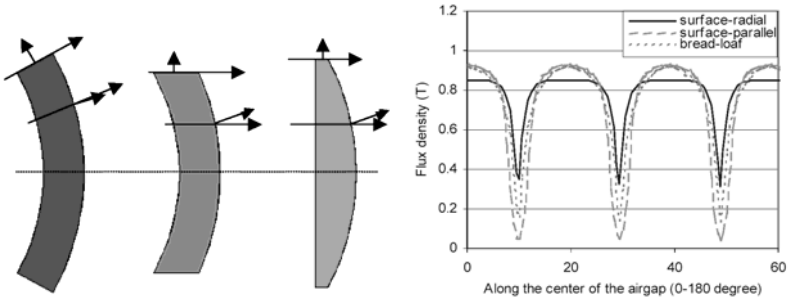

(a) (b)

Figure 10.14. PM shapes (a) and their airgap flux density (b) [6]

The cogging torque may be calculated, within FEA by the coenergy method or by the Maxwell stress tensor method.

There is also a relationship between the e.m.f. harmonics content and the cogging torque as evident in Table 10.1 for the same Ns = 27 slot, 2p = 6 pole PMSM and surface radial (SR), surface parallel (SP) and bread-loaf (BL) shape PMs (Figure 10.14).

Table 10.1 Cogging torque and e.m.f. harmonics [6]

PM shape	Tcoggpp (mNm)	Line to line emf at 1000 rpm [RMS]		
		1^{st} (V)	5^{th} (V)	7^{th} (V)
SR	47.88	2.857	0.05604	0.012256
SP	15.63	2.8681	0.00648	0.008132
BL	5.562	2.8691	0.03459	0.004897

While the emf fundamental and consequently the electromagnetic torque for given sinusoidal current would be the same for all three shapes, the cogging torque is notably smaller for the bread-loaf PMs. The e.m.f. waveform and cogging torque versus position curves depend also on the number of slots per pole per phase q. For q=1 (N_s=24, $2p_1$=8 poles) the e.m.f., cogging torque and electromagnetic torque for sinusoidal current are all shown in Figure 10.15.

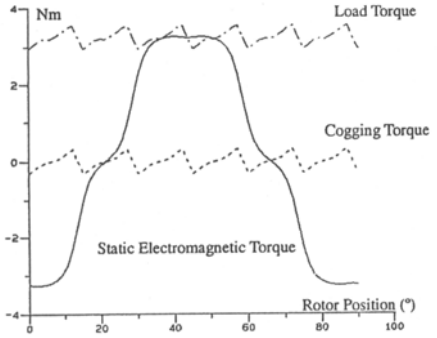

Figure 10.15. E.m.f., cogging torque, total torque (for N_s=24, $2p_1$=8 poles) versus rotor position for sinusoidal current [7]

It is evident that the number of cogging torque fundamental periods N is the lowest common multiplier of N_s and 2p:

$$N = LCM(N_s, 2p) \tag{10.114}$$

The larger N, the smaller the peak value of cogging torque. In the case on Figure 10.15, $N = N_s = 24$.

There are applications such as automotive power steering where the total torque pulsations should be well less than 1% of peak electromagnetic torque of the motor.

Torque pulsations include cogging torque but also refer to e.m.f. and current time harmonics; magnetic saturation of the magnetic circuit plays an important role [6].

Among the many ways to reduce the cogging torque we mention here:

- A higher N = LCM (N_s, 2p)
- PM shape and span optimization (Figure 10.16)
- Rotor or stator skewing (the electromagnetic torque is also reduced)

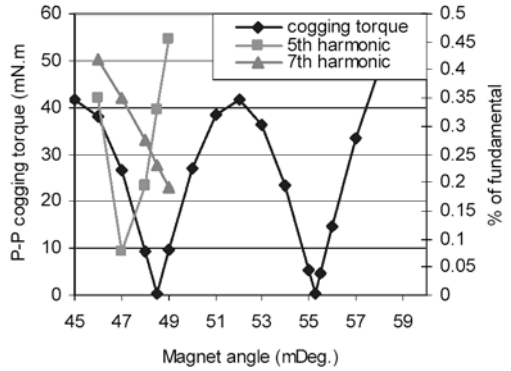

Figure 10.16. Cogging torque and line e.m.f. harmonics content with PM angle for surface PM rotor poles (N_s, 2p=6)

There are two PM span angles for which the cogging torque is zero; the e.m.f. harmonics are not zero for those situations, but also small.

The slot-wound stator windings have been introduced to reduce stator cogging losses by reducing the end-connection length and to reduce the copper torque by increasing the value of N = LCM (N_s, 2p). They may also be called factionary windings as q (slot/pole/phase) < 1.

They may be built in one layer or two layers (Figure 10.18).

Table 10.2 Winding factor / single layer winding [8]

Q	p 2	4	6	8	10	12	14	16
3	*	*	*	*	*	*	*	*
6	*	**0,866**	*	0,866	0,500	*	*	*
9	*	0,736	**0,667**	**0,960**	0,960	0,667	0,218	0,177
12	*	*	*	0,866	**0,966**	*	**0,966**	0,866
15	*	*	0,247	0,383	0,866	0,808	0,957	0,957
18	*	*	*	0,473	0,676	**0,866**	0,844	**0,960**
21	*	*	*	0,248	0,397	0,622	0,866	0,793
24	*	*	*	*	0,430	*	0,561	0,866

Table 10.3 Winding factor/double layer winding [8]

Q	p 2	4	6	8	10	12	14	16
3	**0,866**	0,866	*	*	*	*	*	*
6	*	**0,866**	*	0,866	0,500	*	*	*
9	*	0,617	**0,866**	**0,945**	**0,945**	0,764	0,473	0,175
12	*	*	*	0,866	0,933	*	0,933	0,866
15	*	*	0,481	0,621	0,866	**0,906**	**0,951**	**0,951**
18	*	*	*	0,543	0,647	0,866	0,902	0,931
21	*	*	*	0,468	0,565	0,521	0,866	0,851
24	*	*	*	*	0,463	*	0,760	0,866

Table 10.4 Dimension and proprieties of the 2 layer winding 6 slot/4 pole PMSM

Parameter	value	unit
Topology	Inner rotor IPMSM	
Number of phases	3	-
Number of stator slots	6	-
Number of rotor poles	4	-
Geometry		
Stator outer diameter	56	mm
Stator inner diameter	28	mm
Airgap (minimal)	0.5	mm
Stack length	45	mm
Magnet width	12	mm
Magnet height	3.5	mm
Winding		
Nb. slots/pole/phase	0.5	-
Nb. winding layer	2	-
Nb. turns per phase	20	-
Materials		
Core material	M800-50A	
Magnet type	NdFeB (1.2 T)	

The e.m.f. waveform and cogging torque of a 6/4 slot/pole combination PMSM is shown in Figure 10.17. The e.m.f. is almost sinusoidal. The complete geometrical data are given in Table 10.4 [9].

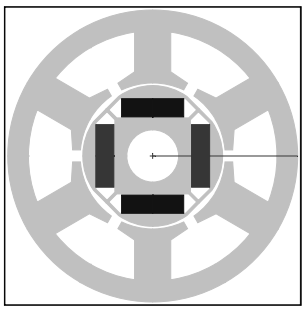

(a) Cross-section of IPMSM

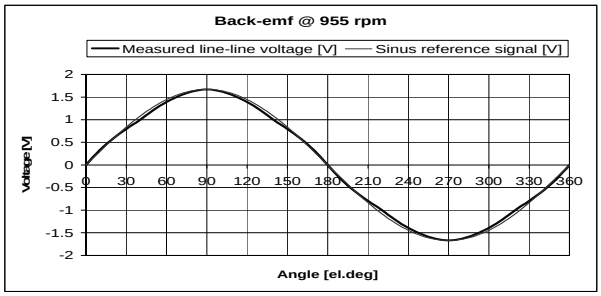

(b) Shape of the back e.m.f. at 955 rpm

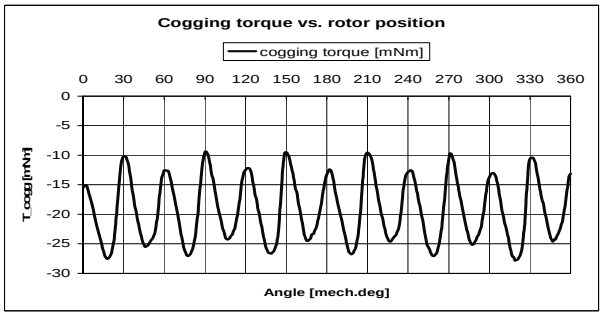

(c) Cogging torque vs. rotor position angle

Figure 10.17. E.m.f. of a 2 layer winding 6 slot/ 4 poles PMSM

Despite the fact that the PM airgap flux density has a rather rectangular distribution in the airgap the e.m.f. may be rather sinusoidal by geometrical optimization, either with surface PM or with interior PMs on the rotor [9].

It is also feasible to produce a trapezoidal e.m.f. waveform, in general, for unilayer windings with nonuniform slots [9, 10].

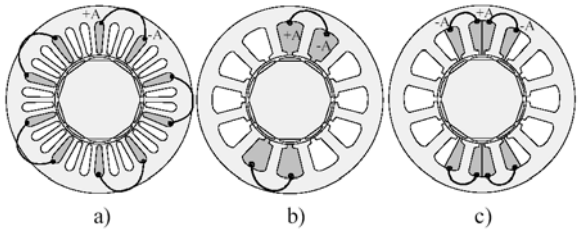

Figure 10.18. Windings for a $2p_1 = 10$ pole machine: a) conventional: $N_s = 30$, $q = 0.4$, b) one layer tooth wound: $N_s = 12$, $q = 0.4$, c) two layer tooth-wound, $N_s = 12$, $q = 0.4$

To secure a large enough e.m.f. fundamental the winding factor K_{w1} should be large enough (> 0.866).

For fractionary q and N_s / 2pm = z/n slots/pole/phase, the space harmonics that occurs with these windings are:

$$\nu = \pm\frac{1}{n}(2mg + 2); g = 0,\pm1,\pm2,\pm3$$ - for n an even number;

$$\nu = \pm\frac{1}{n}(2mg + 1); g = 0,\pm1,\pm2,\pm3$$ - for n an odd number.

Integer and fractionary (sub)harmonics may be present.

The magnetomotive force (m.m.f.) space harmonics produce additional components in the linkage inductance of the slot-wound PMSM while subharmonics may also produce torque pulsations of low frequency.

Double layer such windings are known to having lower subharmonics.

The fundamental winding – factor for some main stator slot N_s, pole number $2p_1$ combinations for single layer and double layer slot-wound PMSMs are shown in Tables 10.2, 10.3.

Consequently slot-wound PMSM, not only enjoy larger efficiency (because of shorter coil end-turns) but also may be controlled for either sinusoidal current or for rectangular current.

They are already applied in industry, from hard disks to servodrives, automotive wheel steering or low speed high torque motor/generators.

Note: Other nonoverlapping coil winding PM brushless motor configurations have been proposed recently but have not reached the markets yet.

They are:

- Transverse flux PM brushless machines (TFM) [11, 12, 13] (with ring shape coil for a large number of poles)
- Claw pole stator composite magnetic core PM brushless machines [14] to cut the manufacturing costs in small motors.

- Flux reversal PM brushless machines (FRM) [15] with standard laminations and stator PMs (in general) to cut manufacturing costs in medium – large torque low speed applications.
- Axial - airgap PMSM, have been introduced to increase torque / volume for various applications [16].

10.9. THE SINGLE-PHASE PMSM

For low power (say below 500 W) home and automotive actuator applications, the single phase PMSM is sometimes used in order to cut the costs of the power electronics converter for variable speed, by reducing the number of power switches.

A typical cylindrical type single phase PMSM is shown in Figure 10.19.

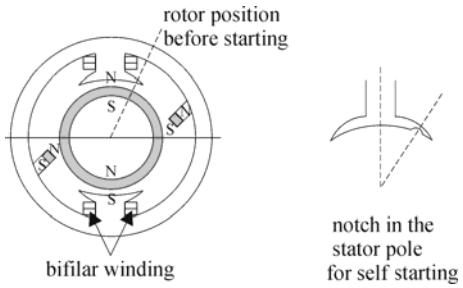

Figure 10.19. Single phase PMSM with bifilar stator winding.

The stator magnetic core is made of silicon laminations (0.5 mm or less in thickness).

There are two semicoils for the positive polarity of current and other two semicoils for the negative polarity of current. The bifilar winding is thus obtained. Though it leads to an increase of copper losses it allows for a low power switch count controller (Chapter 11).

The 2 slot / 2 pole configuration leads to a 2 period cogging torque per revolution.

The machine will not start as the initial position sees the PMs aligned to the stator poles where the electromagnetic (interaction) torque is zero.

To produce a nonzero electromagnetic torque position a few solutions may be applied: a parking magnet pair is placed off-settled between the main poles (Figure 10.11) or a notch is placed asymmetrically on the stator pole towards airgap; alternatively, a stepped airgap under the stator pole solution may be applied.

In all cases only motion in one direction is provided. But once the motor has started in one direction it may be braked and then moved eventually into the opposite direction based on a Hall proximity sensor signal (Chapter 10), if the PEC allows for AC current in the phase coils.

10.10. STEADY STATE PERFORMANCE OF SINGLE PHASE PMSM

At least for sinusoidal e.m.f., the single phase PM brushess motor is, in fact, a synchronous machine. So all the equations already developed in this chapter apply here, but for a single stator electric circuit.

For steady state the phasor form of stator voltage equation is straightforward:

$$\underline{V}_s = R_s \underline{I}_s + \underline{E}_s + j\omega L_s \underline{I}_s ; \underline{E}_s = j\omega_r \lambda_{PM} \tag{10.115}$$

With a sinusoidal e.m.f. E_s:

$$E_s(t) = E_{s1} \cos(\omega_r t) \tag{10.116}$$

and V_s, I_s, stator voltage and current, L_s – stator inductance (independent of rotor position for surface PM rotors), λ_{PM} – the PM flux linkage, R_s – in the stator resistance.

For steady state:

$$I_s(t) = I_{s1} \cos(\omega_r t - \gamma) \tag{10.117}$$

The electromagnetic (interaction) torque is:

$$T_e = p\frac{E_s(t)I(t)}{\omega_r} = \frac{p_1}{\omega_r}\frac{E_{s1}I_{s1}(t)}{2}\left(\cos\gamma + \cos(2\omega_r t - \gamma)\right) \tag{10.118}$$

As for the single phase IM or for the AC brush motor the electromagnetic torque pulsates at double stator current frequency (speed).

Now the cogging torque, with $N_s = 2$ slots, $2p = 2$ poles, has $N = LCM(2, 2) = 2$ periods:

$$T_{cogg} \approx T_{cog\,max} \cos(2\omega_r t - \gamma_{cog}) \tag{10.119}$$

It may be feasible that with such a cogging torque variation to secure $\gamma_{cog} = \gamma$ and, for a certain load torque:

$$T_{cog\,max} = -\frac{pE_{s1}I_{s1}}{2\omega_r} \tag{10.120}$$

This way the torque pulsations are cancelled (the large cogging torque (10.120) may be used for rotor parking at a proper angle to secure safe starting).

At lower load, pulsations occur into the total torque as their complete elimination is performed only for the rated load.

The phasor diagram that corresponds to equation (10.115) is shown in Figure 10.20.

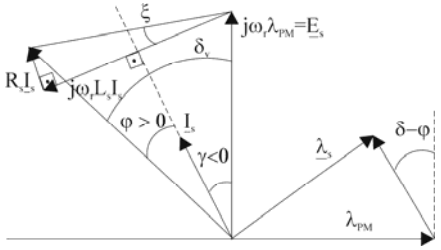

Figure 10.20. The steady state phasor diagram of the single phase PMSM

The core losses p_{iron} may be expressed as proportional to speed and stator flux squared:

$$p_{iron} \approx \frac{\omega_r^2 \lambda_s^2}{P_{iron}} \tag{10.121}$$

R_{iron} may be measured or calculated at the design stage.

In general the copper losses are larger than the iron losses and may be calculated afterwards and added to the efficiency formula.

To calculate the steady state performance for given voltage power angle δ_v, stator voltage V_{s1} and ω_r ($E_s = \omega_r \lambda_{PM}$ – given also) we obtain:

$$I_s = \frac{\sqrt{V_s^2 + E_s^2 - 2V_s E_s \cos\delta_v}}{Z} \tag{10.122}$$

$$Z = \sqrt{R_s^2 + j\omega_r^2 L_s^2}\,; \tan\varphi = \frac{R_s}{\omega_r L_s}; \cos(\varphi + \xi) = \frac{E}{I \cdot Z}\sin\delta_v \tag{10.123}$$

$$\lambda_s^2 = \lambda_{PM}^2 + L_s^2 i_s^2 - 2\lambda_{PM} L_s i_s \cos(\delta_v - \varphi) \tag{10.124}$$

The mechanical power P_{mec} is:

$$P_{mec} \approx V_s I_s \cos\varphi - I_s^2 R_s - \frac{\omega_r^2 \lambda_s^2}{R_{core}} - p_{mec} \tag{10.125}$$

P_{mec}= mechanical losses.

Efficiency η is:

$$\eta = \frac{P_{mec}}{V_s I_s \cos\varphi} \tag{10.126}$$

The electromagnetic torque Te versus power angle for a 150 W single phase PMSM is shown in Figure 10.21 in P.U. for zero and nonzero stator resistance R_s.

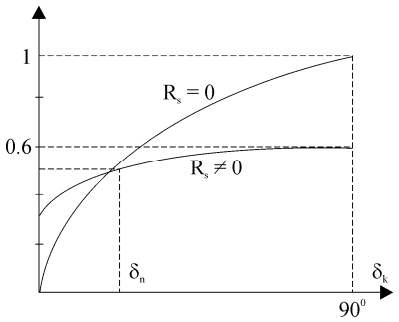

Figure 10.21. Torque versus power (voltage) angle

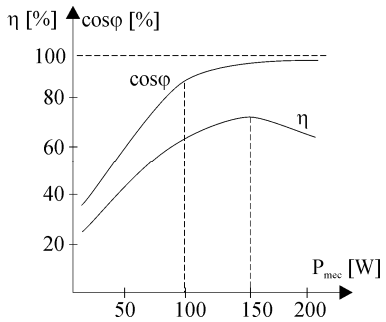

Figure 10.22. Efficiency and power factor versus output power P_{mec} (W)

It is evident that the stator resistance should not be neglected because otherwise the peak torque (at $\delta_v = 90°$) is grossly overestimated.

In V/f scalar control variable speed drives the torque should not surpass the real peak torque, but better be notably smaller (by 30 – 40%) to secure rather stable operation to moderate load torque perturbation. Typical efficiency and power factor curves for a 150 W motor [17] show mildly good performance (Figure 10.22).

Example 10.5:

A single phase PMSM is fed at Vsn = 120 V (RMS) at the frequency f_1= 60 Hz and has two rotor poles 2p = 2. At the corresponding speed, the no load voltage E_s, when the motor is driven by a drive is: E_s=0.95V_{sn}. The stator resistance R_s= 5 Ω and the stator inductance L_s= 0.05 H. Calculate:

a) The speed at f_1= 60 Hz;

b) The stator current for δ_v= 0,45^0, 90^0.

c) The power factor versus δ_v.

d) The average torque for the voltage power angle δ_v=0,45°, 90°, with core and mechanical losses neglected.

Solution:

a) The speed n is:

$$n = f_1/p = 60/1 = 60 \text{ rps} = 3600 \text{ rpm}$$

b) The stator current from (10.122) is:

$$I_s = \frac{\sqrt{V_s^2 + E_s^2 - 2V_sE_s\cos\delta_v}}{Z} =$$

$$= \sqrt{120^2 + (120\cdot 0.95)^2 - 2\cdot 120\cdot 120\cdot 0.95\cdot\cos\delta_v} =$$

$$= \begin{cases} 18/19.5 = 0.92\text{A}, & \delta_v = 0 \\ \dfrac{86.583}{19.5} = 4.44\text{A}, & \delta_v = 45° \\ \dfrac{157.49}{19.5} = 8.07, & \delta_v = 90° \end{cases}$$

$$\text{with : } Z = \sqrt{5^2 + (2\pi 60\cdot 0.05)^2} = 19.5\Omega$$

c) The power factor angle φ comes from (10.123) with:

$$\xi = \tan^{-1}\frac{R_s}{\omega_r L_s} = \tan^{-1}\frac{5}{377\cdot 0.05} = 14.38°$$

$$\cos(\varphi + \xi) = \frac{E_s}{Z\cdot I_s}\sin\delta_v$$

For δ_v=0: $(\varphi+\xi) = 90°$, $\varphi = 90 - 14.38 = 75.32°$;
δ_v=45°: $\cos(\varphi+\xi) = 0.833, (\varphi+\xi) = 33.6°$, $\varphi = 33.6 - 14.38 = 19.20°$;
δ_v=90°: $\cos(\varphi+\xi) = 0.648, (\varphi+\xi) = 49.59°$, $\varphi = 49.59 - 14.38 = 35.21°$;

d) The electromagnetic torque T_e is:

$$Te = \frac{pE_sI_s\cos(\delta_v - \varphi)}{\omega_r} =$$

$$\begin{cases} \delta_v = 0, Te = \dfrac{1}{377}102\cdot 0.92\cdot\cos(0 - 75.62) = 0.0618\text{Nm} \\ \delta_v = 45°, Te = \dfrac{1}{377}102\cdot 4.44\cdot\cos(45 - 19.20) = 1.0815\text{Nm} \\ \delta_v = 90°, Te = \dfrac{1}{377}102\cdot 8.07\cdot\cos(90 - 35.21) = 1.2589\text{Nm} \end{cases}$$

From δ_v=45° to δ_v=90° the torque increases by less than 25%, in part due to the stator resistance presence (the increase would be 30% with zero resistance).

10.11. SUMMARY

- Synchronous motors (SMs) are, in general, three-phase AC motors with DC excited or PM excited or variable reluctance rotors.
- Because the stator m.m.f. travels along the periphery with a speed $n_1 = f_1 / p$ (f_1 - stator frequency, p - pole pairs), the rotor will rotate at the same speed as only two m.m.f.s at relative standstill to produce nonzero average torque.
- Changing the speed means changing frequency.
- Excited rotor SMs require copper-rings and brushes to be connected to a DC controlled power supply. Alternatively, a rotary transformer with diodes on the rotor (secondary) side may provide for brushless energization of the excitation (field) windings.
- From all variable frequency-fed SMs only excited rotor SMs, fed from current-source PECs (as shown in Chapter 14) have a squirrel cage on the rotor, to reduce the machine commutation inductance.
- Unity or leading power factor operation at variable speed and torque is possible only with excited-rotor SMs based on continuous field current control, to nullify the input reactive power to the machine. For this case, if the stator flux is also constant, the speed/torque curve becomes linear, as for a DC brush motor with separate excitation. Flux weakening is performed above base speed.
- PM-rotor SMs may be operated at variable speeds by their control in d-q orthogonal axes coordinates, through adequate coordination of i_d-i_q relationship with torque and speed requirements. Negative (demagnetizing) i_d is required for positive reluctance torque as $L_d < L_q$.
- Multiple flux barrier rotors with conventional or axial laminations, eventually with PMs in axis q (of highest reluctance, $L_d > L_q$), have been shown to produce power factors and efficiencies similar to those of induction machines in the same stator.
- The d-q (space-phasor) model of SMs seems the most adequate vehicle for the design and analysis of variable speed drives with SMs.
- To reduce copper losses and frame size tooth wound PMSMs have been introduced for various applications: from hard disks, through industrial servodrives to active power steering.
- Single phase PMSM are recommended for low power, low system cost home appliance or automotive electric actuation technologies.
- The next chapter will deal only with PM and reluctance SM drives — low and medium powers (up to hundreds of kW), fed from PWM-IGBT converters. Large power industrial drives with excited rotor SMs will be treated in Chapter 14 as they require special PECs.

10.12. PROBLEMS

10.1. A PM-SM with interior PMs ($L_d < L_q$) is fed with a step voltage along the q axis, ΔV_q, while V_d = constant and the speed is constant. Using (10.34)-(10.35) and Figure 10.5, determine the Laplace form of the current Δi_d, Δi_q and torque responses.

10.2. A PM-SM with surface PMs and $q \geq 2$ has the data: $L_d = L_q = 0.01$H, $r_s = 0.5\Omega$, $p = 2$ (pole pairs), rated current (rms, phase current), no-load voltage (at $n_0 = 1800$rpm), $V_0 = 80$V (rms, phase voltage).
Calculate:

a. The PM flux linkage in the d-q model λ_{PM};
b. The torque at rated current with $i_d = 0$ and the corresponding rated terminal voltage for n = 1800 rpm;
c. The ideal no-load speed for $i_q = 0$ and i_d corresponding to rated current;
d. The torque at rated current and voltage for $n' = 3600$ rpm.

10.3. An RSM has the data: rated voltage $V_n = 120$V (rms, phase voltage), $\omega_{1n} = 120$rad/s, $i_{sn} = 20$A (rms, phase current) and the inductances l_d, l_q in relative units: $l_d = 3$ p.u., $l_q = 0.3$ p.u., $r_s = 0.5$ p.u., $p = 2$ pole pairs.
Calculate:

a. L_d, L_q, r_s in Ω if $l(\text{P.U.}) = L\left(\frac{V_n}{I_n \omega_{1n}}\right)^{-1}$;
b. For $i_d / i_q = \sqrt{L_q / L_d}$ and rated current and voltage determine the base speed ω_b, torque, input power and power factor angle φ_1.
c. Add a PM in axis q (acting against i_q) such that the no-load voltage, at base speed ω_b, $e_0 = 0.15$ and calculate the ideal no-load speed for $i_q = i_{sn}$.

10.13. SELECTED REFERENCES

1. **T.J.E. Miller**, Brushless permanent magnet and reluctance motor drives, OUP, 1989
2. **S.A. Nasar, I. Boldea, L. Unnewehr**, Permanent magnet, reluctance and self-synchronous motors, CRC Press, Florida, 1993.
3. **I. Boldea**, Reluctance synchronous machines and drives, OUP, 1996.
4. **R.P. Deodhar, D.A. Staton, T.M. Jahns, T.J.E. Miller**, Prediction of cogging torque using the flux - m.m.f. diagram technique, IEEE Trans., vol.IA-32, no.3, 1996, pp.569-576.
5. **I. Boldea and S.A. Nasar**, Unified treatment of core losses and saturation in orthogonal axis model of electric machines, Proc.IEE, vol.134, Part.B, 1987, pp.355-363.
6. **M.S. Islam, S. Mir, T. Sebastian, S. Underwood,** "Design consideration of sinusoidal excited permanent magnet machines for low torque ripple applications", Record of IEEE – IAS – 2004, Seattle, USA.
7. **J. Cross, P. Viarouge,** "Synthesis of high performance PM motors with concentrated windings", IEEE Trans. Vol. EC-17, no. 2, 2002, pp. 248-253.
8. **F. Magnussen, C. Sadarangani,** "Winding factors and Joule losses of permanent magnet machines with concentrated windigs", Record of IEEE – IEMDC – 2003, vol. 1, pp. 333-339.

9. **D. Iles – Klumpner, I. Boldea,** "Optimization design of an interior permanent magnet synchronous motor for an automotive active steering system", Record of OPTIM 2004, vol. 2, pp. 129-134.
10. **D. Ishak, Z.Q. Zhu, D. Howe,** "Permanent magnet brushless machines with unequal tooth widths and similar slot and pole numbers", Record of IEEE – IAS – 2004, Seattle, USA.
11. **H. Weh, H. May,** "Achievable force densities for permanent magnet excited machines in new configurations", Record of IEM – 1986, vol. 3, pp. 1107-1111.
12. **E. Henneberger, I.A. Viorel,** Variable reluctance electrical machines, Shaker Verlag, Aachen, 2001.
13. **I. Luo, S. Huang, S. Chen, T. Lipo,** "Design and experiments of a novel axial circumpherential current permanent magnet (AFCC) machine with radial airgap", Record of IEEE – IAS – 2001.
14. **I. Cross, P. Viarouge,** "New structure of polyphase claw pole machines", IEEE Trans. Vol. IA – 40, no. 1, 2004, pp. 113-120.
15. **I. Boldea, I. Zhang, S.A. Nasar,** "Theoretical characterization of flux reversal machine in low speed servodrives – the pole – PM configuration", IEEE Trans. Vol. IA 38, no. 6, 2002, pp. 1549-1557.
16. **M. Cerchio, G. Griva, F. Profumo, A. Tenconi,** "'Plastic' axial flux machines: design and prototyping of a multidisk PM synchronous motor for aircraft applications", Record of ICEMS – 2004, Je Ju Island, Korea.
17. **V. Ostovic,** "Performance comparison of U core and round stator single phase PM motors for pump applications", IEEE Trans. Vol. IA – 38, no. 2, 2002, pp. 476-482.